analytical chemistry

Article

pubs.acs.org/ac

Enhanced Photoelectrochemical Immunosensing Platform Based on CdSeTe@CdS:Mn Core–Shell Quantum Dots-Sensitized TiO_2 Amplified by CuS Nanocrystals Conjugated Signal Antibodies

Gao-Chao Fan,[†,‡] Hua Zhu,[†] Dan Du,[‡] Jian-Rong Zhang,[*,†,§] Jun-Jie Zhu,[*,†] and Yuehe Lin[*,‡]

[†]State Key Laboratory of Analytical Chemistry for Life Science, Collaborative Innovation Center of Chemistry for Life Sciences, School of Chemistry and Chemical Engineering, Nanjing University, Nanjing 210093, People's Republic of China

[‡]School of Mechanical and Materials Engineering, Washington State University, Pullman, Washington 99164, United States

[§]School of Chemistry and Life Science, Nanjing University Jinling College, Nanjing 210089, People's Republic of China

Supporting Information

ABSTRACT: A new, ultrasensitive photoelectrochemical immunosensing platform was established on the basis of CdSeTe@CdS:Mn core–shell quantum dots-sensitized TiO_2 coupled with signal amplification of CuS nanocrystals conjugated signal antibodies. In this proposal, carcinoembryonic antigen (CEA, Ag) was selected as an example of target analyte to show the analytical performances of the platform. Specifically, TiO_2-modified electrode was first assembled with CdSeTe alloyed quantum dots (AQDs) via electrostatic adsorption assisted by oppositely charged polyelectrolyte, and then further deposited with CdS:Mn shells on the surface of CdSeTe AQDs via successive ionic layer adsorption and reaction strategy, forming TiO_2/CdSeTe@CdS:Mn sensitization structure, which was used as photoelectrochemical matrix to immobilize capture CEA antibodies (Ab_1); signal CEA antibodies (Ab_2) were labeled with CuS nanocrystals (NCs) to form Ab_2–CuS conjugates, which were employed as signal amplification elements when specific immunoreaction occurred. The ultrahigh sensitivity of this immunoassay resulted from the following two aspects. Before detection of target Ag, the TiO_2/CdSeTe@CdS:Mn sensitization structure could adequately harvest the exciting light with different bands, evidently expedite the electron transfer, and effectively depress the charge recombination, resulting in noticeably increased photocurrent. When target Ag existed, the Ab_2–CuS conjugates could dramatically decrease the photocurrent due to competitive absorption of exciting light and consumption of electron donor for CuS NCs coupled with steric hindrance of Ab_2 molecules. The fabricated photoelectrochemical immunosensor showed a low limit of detection of 0.16 pg/mL and a wide linear range from 0.5 pg/mL to 100 ng/mL for CEA detection, and it also exhibited good specificity, reproducibility, and stability.

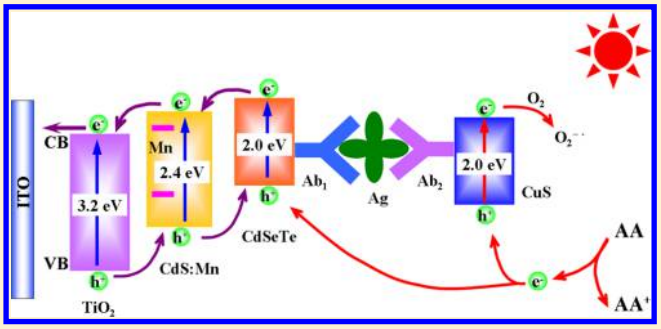

As a rapidly developed and promising analytical technique for the detection of biomarkers, photoelectrochemical immunoassay has attracted widespread research interest, because it has distinct advantages of simple devices, low price, simple operation, and easy micromation and integration, which is well-suited for rapid, real-time, and high-throughput biological analysis.[1,2] Furthermore, it possesses potentially higher sensitivity due to different forms of energies for the detection signal and excitation source, causing the obviously reduced background signal.[3,4] Undoubtedly, photoactive species play a very important role in analytical performances of the photoelectrochemical immunosensors. Up to now, the most popular utilized photoactive species belong to n-type inorganic semiconductor nanomaterials or quantum dots.[5−9] Recently, nano TiO_2 has proved to be an excellent base material to develop photoelectrochemical immunoassays because of its biocompatibility, photoelectric activity, high stability, environmental safety, and low cost.[10−12] However, the large band gap of TiO_2 (~3.2 eV) limited its direct applications, because it could absorb only the ultraviolet light (<387 nm), leading to poor utilization of light energy. CdS is an often-used semiconductor with a band gap of 2.4 eV corresponding to the optimal absorption range of middle-wavelength light (<520 nm).[13] To depress the charge recombination, metal ions of Mn^{2+} are usually introduced into CdS to form CdS:Mn doping structure, because the lifetime of charge recombination for CdS:Mn is much longer than that of CdS.[14] As compared to binary semiconductor quantum dots, the ternary alloyed structure owns unique electronic and optical properties, because the absolute energy values of conduction and valence bands can be accurately adjusted not only by particle size but also by alloying composition.[15−17] Thereinto, CdSeTe alloyed

Received: January 12, 2016
Accepted: February 24, 2016
Published: February 24, 2016

ACS Publications © 2016 American Chemical Society

DOI: 10.1021/acs.analchem.6b00144
Anal. Chem. 2016, 88, 3392−3399

Scheme 1. Construction Process of the Proposed Photoelectrochemical Immunosensing Platform

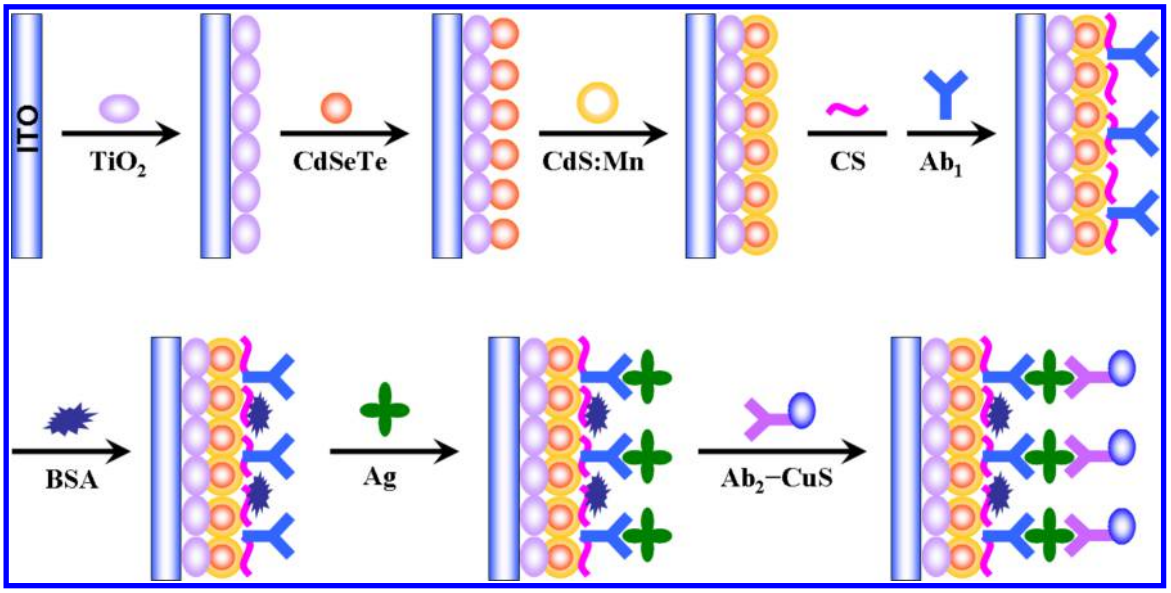

quantum dots possess a lower band gap than CdS,[18,19] which corresponds to the optimal absorption range of long-wavelength light. Because different semiconductors have different optimal absorption regions due to their different band gaps, coupling of TiO_2 with narrow band gap semiconductors to produce sensitization structure with cascade band-edge levels is very effective for photoelectrochemical immunosensors to enhance the light absorption efficiency, promote the electron transfer, and prolong the lifetime of charge carriers.

According to a comprehensive literature survey, the majority of highly sensitive photoelectrochemical immunoassays belong to signal-off type, because specific biorecognition between antibody and antigen would produce an insulating and hydrophobic layer on the electrode surface, which blocks the electron transfer. So far, the amplification methods for signal-off photoelectrochemical immunoassays mainly associate with enzymatic reactions and steric-hindrance effects.[20−23] Yet, the application of enzymes evidently increased the cost of sensor fabrication and complicated the testing procedure; the introduction of large-sized insulating substances obviously weakened the water solubility of the labeled signal antibodies and narrowed the linear range of detection. Hence, other simple but effective signal amplification methods would surely be desirable. In recent years, copper sulfide (CuS) nanomaterials have exhibited potential applications in the fields of solar cells,[24,25] photocatalysis,[26] supercapacitors,[27] optical limiters,[28] lithium ion batteries,[29] and biosensors[30,31] due to favorable electrical, optical, and super ionic properties. CuS is a p-type semiconductor with a band gap value of 2.0 eV, and it can effectively absorb the middle-wavelength light. Under light excitation, the photogenerated electrons in p-type CuS are captured by electron acceptors (such as dissolved oxygen), and the photogenerated holes have strong oxidizability to electron donors.[32] When CuS nanocrystals (NCs) are labeled on signal antibodies (Ab_2) to form Ab_2−CuS conjugates, the photocatalytic property of CuS would competitively absorb the exciting light and consume the electron donor of the photoelectrochemical system, resulting in evidently weakened photocurrent intensity. Meanwhile, the steric hindrance of Ab_2 molecules also leads to the reduced photocurrent intensity of the immunosensing system. As CuS NCs and Ab_2 molecules synergistically promote the decrease of photocurrent signal, excellent analytical performance of the photoelectrochemical immunoassays can be achieved by employing Ab_2−CuS conjugates as signal amplification elements. However, up to the present, this novel and effective amplification method has not been explored in any of the photoelectrochemical immunoassays.

We herein present an enhanced, promising photoelectrochemical immunosensing platform based on CdSeTe@CdS:Mn core−shell quantum dots-sensitized TiO_2 coupled with signal amplification of CuS nanocrystals (NCs) conjugated signal antibodies (Ab_2), as displayed in Scheme 1. Experimentally, carcinoembryonic antigen (CEA, Ag) was used as a model of target analyte to illustrate the diversity of the proposed platform. First, TiO_2 nanoparticles were covered on a bare indium−tin oxide (ITO) electrode, and the mesoporous film was produced after being treated in high temperature. The ITO/TiO_2 electrode was assembled with CdSeTe cores via electrostatic adsorption assisted by oppositely charged polyelectrolyte and subsequently coated with CdS:Mn shells by successive adsorption and reaction of Cd^{2+}/Mn^{2+} and S^{2-}, forming CdSeTe@CdS:Mn core−shell quantum dots-sensitized TiO_2 to significantly increase the photocurrent response. Next, CEA capture antibodies (Ab_1) were immobilized on the electrode via the assistance of linking molecules of chitosan (CS). After bovine serum albumin (BSA) blocked unbound sites of the Ab_1-modified electrode, the immunosensor was ready. For target Ag detection, varied concentrations of Ag were first immobilized on the sensing electrode by specific immunoreaction between Ab_1 and Ag, and then the fixed concentration of Ab_2−CuS conjugates as signal amplification elements was further immobilized via specific immunoreaction between Ag and Ab_2, resulting in a noticeably weakened photocurrent response. The designed photoelectrochemical sandwich immunoassay presented ultrahigh sensitivity, and good reproducibility, specificity, and stability.

EXPERIMENTAL SECTION

The materials and reagents, and apparatus utilized in this work were described in the Supporting Information.

DOI: 10.1021/acs.analchem.6b00144
Anal. Chem. 2016, 88, 3392−3399

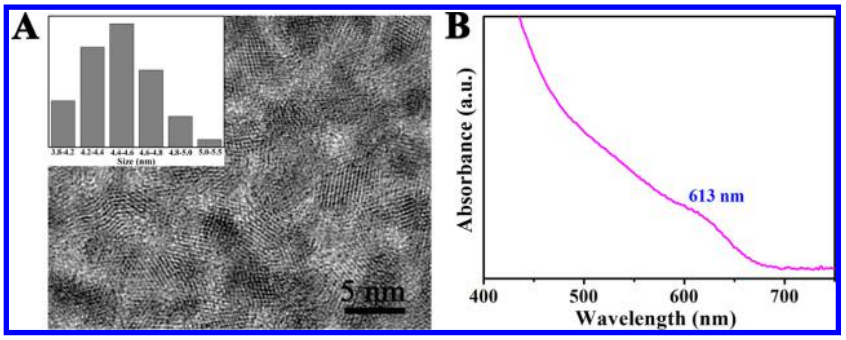

Figure 1. (A) HRTEM image and (B) UV−vis absorption spectrum of the synthesized CdSeTe AQDs. Inset of panel A: Size distribution of the CdSeTe AQDs.

Synthesis of CdSeTe AQDs. The synthetic process of water-soluble CdSeTe alloyed quantum dots (AQDs) originated from the previous work.[33] Typically, 0.6 mmol of $CdCl_2$ and 1.02 mmol of 3-mercaptopropionic acid (MPA) were mixed in a 120 mL solution in a three-necked flask, and the pH value of the solution was regulated to 11.8 by adding 1.0 M NaOH under stirring. After the solution was deaerated with highly pure N_2 for 30 min, 120 mg of $NaBH_4$ and 12 mg of Na_2TeO_3 were successively added in. When the mixture solution was heated to 100 °C, 0.5 mL of 12 mM freshly prepared NaHSe solution was immediately injected. The typical molar ratio of $Cd^{2+}/(Te^{2-}+Se^{2-})$/MPA was 1/0.1/1.7, and the molar ratio of Te/Se was 9/1. The resulting mixture was kept at 100 °C and refluxed for 1 h under N_2 protection, and finally the desired CdSeTe AQDs solution was obtained.

Fabrication of the ITO/TiO_2/CdSeTe@CdS:Mn Electrode. Prior to modification, ITO electrodes were ultrasonically cleaned in acetone, 1 M NaOH of ethanol/water mixture (volume ratio of 1:1), and deionized (DI) water for 15 min in order, and then were dried at 100 °C for several hours. Next, 8 mg of TiO_2 powder was scattered in 8 mL of DI water ultrasonically, and then 20 μL of this uniformly distributed suspension (1.0 mg/mL) was dropped on an ITO electrode with a premodified area of 0.25 cm^2. After being dried, the electrode was treated at 450 °C for 30 min in air and then naturally cooled to the room temperature. The CdSeTe AQDs were assembled by first immersing the ITO/TiO_2 electrode into a 1% positively charged poly(diallyldimethylammonium chloride) (PDDA) solution for 30 min and then into the CdSeTe AQDs solution for 1 h. After each immersing step, the film was carefully rinsed with DI water. The modification of CdS:Mn shells on the surface of CdSeTe AQDs was according to successive ionic layer adsorption and reaction (SILAR) strategy.[34] The ITO/TiO_2/CdSeTe electrode was first immersed into 0.1 M $Cd(NO_3)_2$ mixed with 0.08 M $Mn(Ac)_2$ methanol solution for 5 min, and then immersed into 0.1 M Na_2S water/methanol mixture (volume ratio of 1:1) for 5 min. After each immersion step, the electrode was rinsed with methanol. This SILAR cycle was repeated six times, and the desired ITO/TiO_2/CdSeTe@CdS:Mn electrode was obtained.

Synthesis of CuS NCs and Ab_2−CuS Conjugates. Water-soluble CuS NCs were synthesized according to our previous literature method.[35] Typically, 6 μL of thioglycolic acid (TGA) was injected into 20 mL of 2 mM $Cu(NO_3)_2$ solution, and the pH value of this solution was regulated to 9.0 with 0.5 M NaOH. After being deaerated with highly pure N_2 for 30 min, 5 mM Na_2S solution was dropwise mixed in the above solution to make the molar ratio of Na_2S to $Cu(NO_3)_2$ about 2.5. The resulting solution was allowed to react under N_2 protection for 24 h at room temperature, and a deep brown colloid solution was acquired. After being centrifuged and washed with ethanol and DI water several times, the product was obtained, and it was redispersed in DI water again to form CuS NCs solution.

The synthetic procedure of Ab_2−CuS conjugates was described as below. 200 μL of 10 mg/mL newly prepared EDC solution was first mildly mingled with 1 mL of CuS NCs suspension (0.2 mg/mL) for 30 min at room temperature. After centrifugation to remove the supernatant liquid, 1 mL of Ab_2 solution (200 μg/mL) was added and incubated for 12 h under shaking at 4 °C. After being centrifuged and washed with phosphate buffer solution (PBS) several times, the desired Ab_2−CuS conjugates were acquired and dispersed to 1 mL by 10 mM of PBS (pH 7.4).

Construction of the Immunoassay. The construction procedure of the immunosensor was based on our previous work.[36] 15 μL of 0.1 wt % chitosan (CS) solution containing 1% acetic acid was covered onto the ITO/TiO_2/CdSeTe@CdS:Mn electrode surface and was dried at 50 °C. While the electrode was rinsed with 0.1 M NaOH and DI water in order, 20 μL of 5% glutaraldyhyde was scattered onto the electrode surface and maintained for 30 min. The unbound or physically adsorbed glutaraldyhyde was removed by washing the electrode with DI water. Subsequently, the electrode was covered with 20 μL of 100 μg/mL Ab_1 and allowed to incubate at 4 °C for at least 12 h. After being rinsed with the washing buffer solution (PBS, pH 7.4, 10 mM), the electrode was incubated with 20 μL of 10 mM PBS (pH 7.4) containing 1% (w/v) BSA at 37 °C for 30 min to block nonspecific binding sites and then rinsed with the washing buffer solution thoroughly. Next, 20 μL of different concentrations of target Ag was dropped on the BSA blocked electrode for an incubation of 1 h at 37 °C followed by washing with washing buffer solution. After specific immunoreaction between Ab_1 and Ag, the electrode was allowed for labeling by additional incubation with 20 μL of Ab_2−CuS conjugates solution for 1 h at 37 °C. Eventually, the resulting electrode was washed thoroughly with washing buffer solution and introduced into the photocurrent test.

Photoelectrochemical Measurement. Photoelectrochemical detection was performed at room temperature in PBS (pH 7.4, 0.1 M) including 0.1 M ascorbic acid (AA), which acted as a sacrificial electron donor during measurement of the photocurrent. White light generated by a xenon lamp with a spectral range from 200 to 2500 nm was employed as excitation light source, which was switched on and off every 10 s. The external voltage was 0.0 V.

DOI: 10.1021/acs.analchem.6b00144
Anal. Chem. 2016, 88, 3392−3399

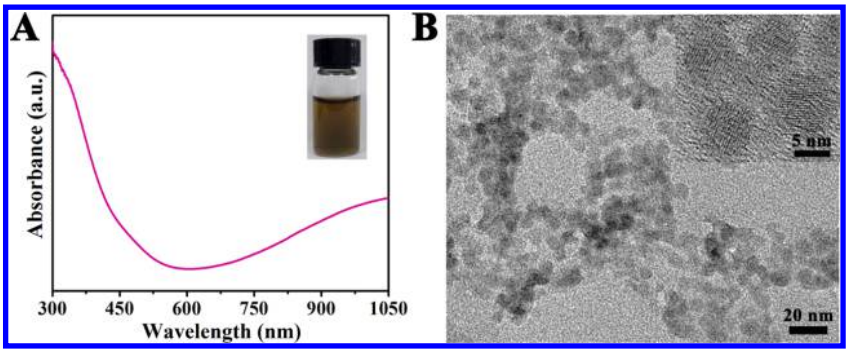

Figure 2. (A) UV−vis absorption spectrum and (B) TEM image of the synthesized CuS NCs. Inset of panel A: Photograph image of the CuS NCs solution after being stored for 2 weeks. Inset of panel B: HRTEM image of the CuS NCs.

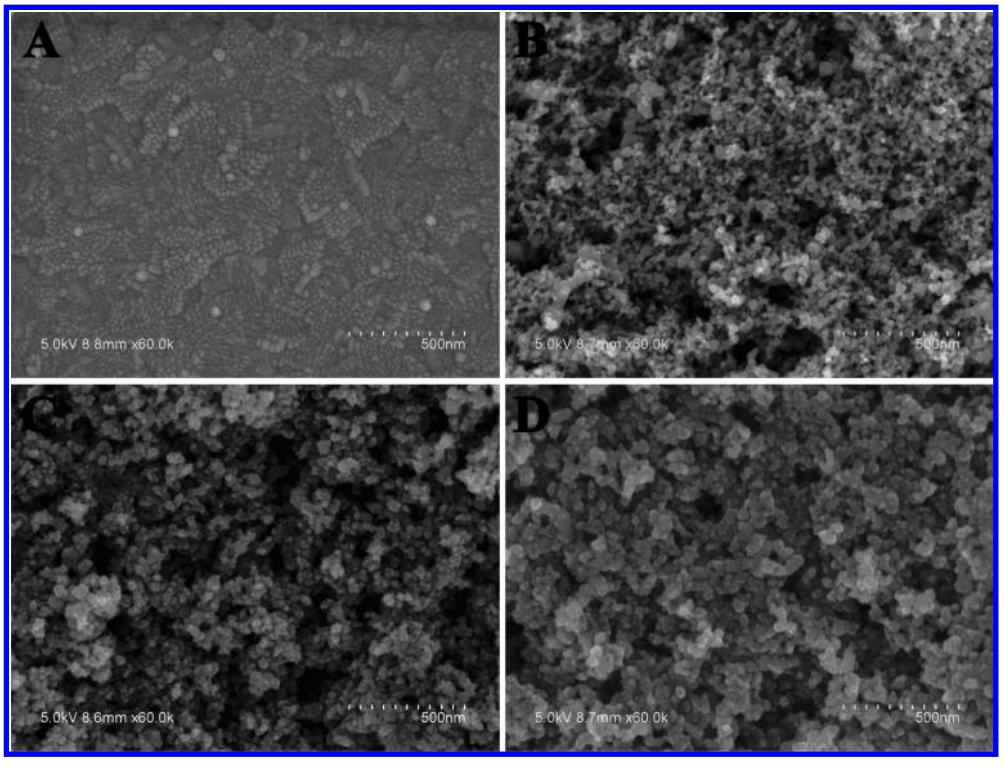

Figure 3. SEM images of the (A) bare ITO, (B) ITO/TiO_2, (C) ITO/TiO_2/CdSeTe@CdS:Mn, and (D) ITO/TiO_2/CdSeTe@CdS:Mn/Ab_1/BSA electrode surfaces.

RESULTS AND DISCUSSION

Characterization of CdSeTe AQDs. The optimization for molar ratio of Te/Se in CdSeTe AQDs was described in the Supporting Information. Panels A and B of Figure 1 present the high-resolution transmission electron microscopy (HRTEM) image and UV−visible (UV−vis) absorption spectrum of the prepared CdSeTe AQDs, respectively. The outline and lattice fringes of the CdSeTe AQDs could be clearly observed in HRTEM image, and the average size of 4.46 nm was acquired from the size distribution in the inset of Figure 1A. The UV−vis absorption spectrum of the CdSeTe AQDs exhibited an obvious absorption peak located at 613 nm and a broad absorption range below 675 nm, which potentially indicated an effective absorption to long-wavelength light. Besides, the band gap value of the CdSeTe AQDs was calculated to be 2.0 eV according to the energy−wavelength relation $E_g = hc/\lambda$, where E_g, h, c, and λ represent band gap, Planck constant, light velocity, and first excitonic peak position, respectively.

Characterization of CuS NCs. Panels A and B of Figure 2 display the UV−vis absorption spectrum and transmission electron microscopy (TEM) image of the synthesized TGA-capped CuS NCs, respectively. As shown in Figure 2A, the spectrum was similar to that of the previously reported CuS materials,[37,38] and it exhibited a short-wavelength absorption edged at about 550 nm. Moreover, it also revealed an increased absorption in the near-infrared region, indicating covellite phase of the obtained products.[39] When the prepared CuS NCs were scattered in water, a uniform deep brown solution was formed, and no precipitates appeared even after 2 weeks (see inset of Figure 2A), indicating good water stability and dispersibility of the CuS NCs. It can be seen from the TEM image (Figure 2B) that the synthesized CuS NCs were spherical particles with relatively uniform morphologies. The HRTEM image was shown in the inset of Figure 2B. From the clear outline and lattice fringes of the CuS NCs, an average diameter of about 6.8 nm could be obtained.

DOI: 10.1021/acs.analchem.6b00144
Anal. Chem. 2016, 88, 3392−3399

Photoelectrochemical Property of the ITO/TiO_2/CdSeTe@CdS:Mn Electrode. Enhanced photocurrent conversion efficiency is highly desirable to a photoelectrochemical immunosensor, because it is closely associated with the sensitivity. To acquire maximum photocurrent intensity of the ITO/TiO_2/CdSeTe@CdS:Mn electrode, optimal preparation conditions were explored, and the detailed descriptions were similar to our previous works.[22,33] Thus, 1 mg/mL TiO_2 suspension, 0.08 M Mn^{2+}, and six SILAR cycles of CdS:Mn were adopted during the fabrication process. The photocurrent intensity of the ITO/TiO_2/CdSeTe@CdS:Mn electrode for each preparation procedure is shown in Figure S2. The ITO/TiO_2 electrode exhibited a relatively small photocurrent, because TiO_2 could harvest only the ultraviolet light resulting in low photocurrent conversion efficiency. After CdSeTe AQDs assembly, the photocurrent intensity was 3.6-fold higher than that of the ITO/TiO_2 electrode, which was because the modified CdSeTe AQDs evidently extended the absorb range to long-wavelength light (~670 nm). After CdS:Mn shells were coated on the surface of the CdSeTe AQDs, the photocurrent intensity further increased to 10.3-fold higher than that of the ITO/TiO_2 electrode, which was because the modified CdS:Mn shells obviously increased the absorption of middle-wavelength light (~570 nm) and also effectively depressed the electron−hole recombination.[34]

SEM Characterization of the Immunosensor. The surface topography of the immunosensing electrode during each preparation procedure was monitored by scanning electron microscopy (SEM) images. Figure 3A−D displays the typical SEM images of the bare ITO, ITO/TiO_2, ITO/TiO_2/CdSeTe@CdS:Mn, and ITO/TiO_2/CdSeTe@CdS:Mn/Ab_1/BSA electrode surfaces, respectively. As shown in Figure 3A, plenty of indium tin oxide clusters were scattered on the bare ITO electrode. It could be seen from Figure 3B that a large amount of TiO_2 spherical nanoparticles with the diameter of 22−28 nm were coated on the electrode surface, and these nanoparticles had formed a mesoporous film. After CdSeTe@CdS:Mn core−shell quantum dots immobilization, as shown in Figure 3C, the particles on the electrode surface became larger and the pores got smaller, which indicated that the CdSeTe@CdS:Mn core−shell quantum dots had successfully adhered on the surface of the TiO_2 nanoparticles. After Ab_1 and BSA were further modified, plenty of larger-sized protein molecules uniformly scattered on the electrode surface and covered almost all of the nanoparticles and pores (Figure 3D). Hence, the SEM characterization indicated successful development of the immunosensing electrode.

EIS Characterization of the Immunoassay. Electrochemical impedance spectroscopy (EIS) is a useful means to characterize interface properties of the electrodes.[40,41] Figure 4 presents the impedance spectra of various electrodes coming from different fabrication procedures. Each impedance spectrum was composed of a semicircle reflecting the electron-transfer limited process and a linear part originated from the diffusion limited process. The electron-transfer resistance (R_{et}) equals the semicircle diameter, which represents the restricted diffusion of the redox probe accessing the layer. For ITO/TiO_2 electrode, the impedance spectrum revealed a relatively small R_{et} (curve a). After CdSeTe@CdS:Mn core−shell quantum dots, Ab_1 and BSA were successively immobilized onto the electrode surface in order, the R_{et} increased gradually due to weak conductivity of semiconductors and insulating property of protein molecules

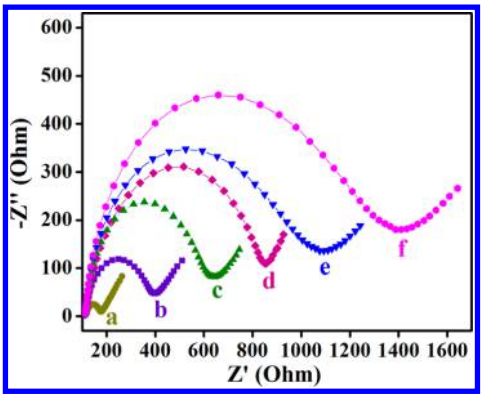

Figure 4. EIS of (a) the ITO/TiO_2 electrode, (b) after CdSeTe@CdS:Mn core−shell QDs modification, (c) after Ab_1 immobilization, (d) after BSA blocking, (e) after incubation with 20 μL of 10 μg/mL Ag, and then (f) further incubation with Ab_2−CuS conjugates.

(curves b−d), suggesting successful fabrication of the immunosensor. After the immunosensor was incubated with target Ag and then Ab_2−CuS conjugates, the R_{et} increased continuously (curves e and f), proving that the immunoreactions between Ab_1 and target Ag as well as target Ag and Ab_2−CuS conjugates had successfully occurred.

Photoelectrochemical Mechanism of the Immunoassay. The photogenerated electron−hole transfer process of the immunoassay was shown in Scheme 2. For TiO_2/CdSeTe@CdS:Mn sensitization structure, the TiO_2 substrate, CdSeTe core, and CdS:Mn shell possessed different energy gaps corresponding to different optimal absorption bands, which adequately utilized the energy of exciting light. Meanwhile, TiO_2, CdS, and CdSeTe presented cascade band-edge levels, which promoted ultrafast transfer of electron−hole pairs and effectively inhibited the charge recombination. Besides, the doped Mn^{2+} in CdS also obviously depressed the electron annihilation, resulting from the formation of a new energy band gap in the middle of CdS. Therefore, the photocurrent response of the immunosensor evidently enhanced. All of these results were demonstrated by photocurrent characterization of the ITO/TiO_2/CdSeTe@CdS:Mn electrode.

For signal amplification elements, Ab_2−CuS conjugates were used to effectively decrease the photocurrent response. It is easy to know that the Ab_2 molecules own obvious steric hindrance, which impeded the electron transfer, leading to reduced photocurrent intensity. More importantly, we herein first utilized p-type CuS NCs as signal-off labels, and two major factors on its photocatalytic property can be concluded to decrease the photocurrent intensity. First, the prepared p-type CuS NCs possessed a broad absorption range (as shown in Figure 2A), which could competitively absorb the light energy, leading to weakened light absorption efficiency for the TiO_2/CdSeTe@CdS:Mn photoelectrochemical matrix. Second, under light excitation, the photogenerated electrons in the conduction band of CuS NCs were captured by O_2 dissolved in AA solution to form $O_2^{-\bullet}$,[42,43] and the holes in the valence band of CuS NCs were neutralized by AA electron donor, leading to reduced concentration of AA for the reaction with the holes generated in the sensitization structure of TiO_2/CdSeTe@CdS:Mn.

Concisely, two main aspects contributed to ultrahigh sensitivity of the proposed immunoassay. Before incubation with target Ag, the immunosensor owned an evident photo-

DOI: 10.1021/acs.analchem.6b00144
Anal. Chem. 2016, 88, 3392−3399

Scheme 2. Photogenerated Electron−Hole Transfer Mechanism of the Immunosensing System for the Detection of Target Ag

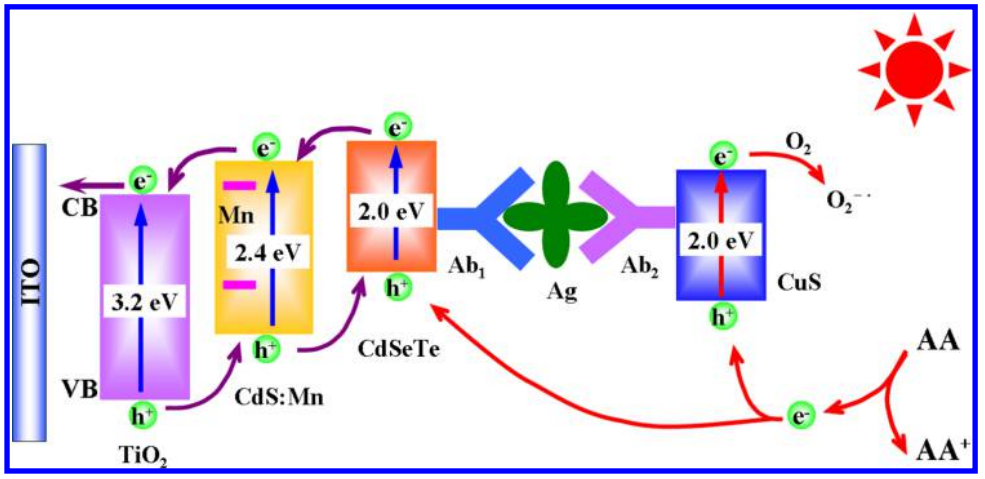

current response, because the TiO_2/CdSeTe@CdS:Mn sensitization structure could adequately absorb the light energy, dramatically promote the electron transfer, and effectively inhibit the electron−hole recombination. While in the presence of target Ag, the Ab_2−CuS conjugates specifically bound on the electrode surface, which evidently weakened the light absorption efficiency, decreased the concentration of AA electron donor, and increased the steric hindrance of the immunosensing electrode, leading to significantly decreased photocurrent response.

Photocurrent Characterization of the Immunoassay. The building process of the immunoassay could also be characterized by photocurrent responses. As displayed in Figure 5, the ITO/TiO_2/CdSeTe@CdS:Mn electrode corresponded

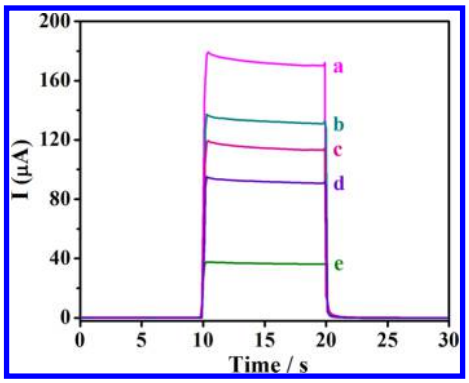

Figure 5. Photocurrent responses of (a) the ITO/TiO_2/CdSeTe@CdS:Mn electrode, (b) after Ab_1 immobilization, (c) after BSA blocking, (d) after incubation with 20 μL of 10 μg/mL Ag, and then (e) further incubation with Ab_2−CuS conjugates.

to a very high photocurrent response (curve a). After Ab_1 and BSA were successively modified on the electrode, the photocurrent intensity gradually reduced (curve b and c), which could be ascribed to evident steric hindrance of these protein molecules. The photocurrent decrease for Ab_1 modification was more obvious due to poor charge-transfer abilities of linking molecules of chitosan and glutaraldyhyde. After the as-fabricated immunosensing electrode was incubated with target Ag and then Ab_2−CuS conjugates, the photocurrent responses decreased to ∼80% and 32% of the initial immunosensing electrode (curves d and e). It was noted that the photocurrent decrement for target Ag immobilization was evidently less than that of the subsequently modified Ab_2−CuS conjugates, which was mainly ascribed to the competitive absorption of exciting light and effective consumption of AA electron donor for the anchored CuS NCs. In addition, bare Ab_2 molecules were also utilized as signal amplification elements to conduct the photoelectrochemical test, and the results revealed that the photocurrent decrement to bare Ab_2 molecules was only about 35% of that to Ab_2−CuS conjugates, demonstrating a distinct advantage of the Ab_2−CuS conjugates as signal amplification elements. Thus, the photocurrent characterization confirmed the formation of the Ab_2−CuS conjugates and successful development of the proposed immunoassay.

Photoelectrochemical Detection for CEA. CEA detection was based on the degree of photocurrent change producing by the sandwich immunoreactions between Ab_1 and target Ag as well as target Ag and Ab_2−CuS conjugates. The photocurrent response of the immunosensor was directly associated with the concentration of target Ag. Figure 6A presents the photocurrent responses of the immunosensor after being incubated with different concentrations of target Ag and then further incubated with fixed concentration of Ab_2−CuS conjugates. As the concentration of target Ag elevated, more of the Ab_2−CuS conjugates specifically bound on the electrode surface to competitively absorb the exciting light, consume the AA electron donor, and hinder the electron transfer, leading to gradually reduced photocurrent intensity. As displayed in Figure 6B, the photocurrent response linearly decreased with increasing logarithm of target Ag concentration in the range from 0.5 pg/mL to 100 ng/mL. The regression equation was $I = 65.30 - 12.25 \log C_{CEA}$ (ng/mL), with a correlation coefficient of 0.9972. The limit of detection (LOD, S/N = 3) for CEA concentration was calculated to be 0.16 pg/mL, which was evidently lower than those of previous methods such as chemiluminescent assay (0.6 ng/mL),[44] amperometric assay (60 pg/mL),[45] potentiometric assay (30 ng/mL),[46] colorimetric assay (2 pM),[47] electrochemiluminescent assay (20 pg/mL),[48] fluorescent assay (5 pg/mL),[49] electrochemical assay (3.5 pg/mL),[50] etc. As compared to previous photoelectrochemical immunoassays developed on the basis of enzyme reactions as well as steric-hindrance effects, as shown in Table S1, the constructed photoelectrochemical immunoassay still possessed a lower or comparable limit of detection. Besides, it

DOI: 10.1021/acs.analchem.6b00144
Anal. Chem. 2016, 88, 3392−3399

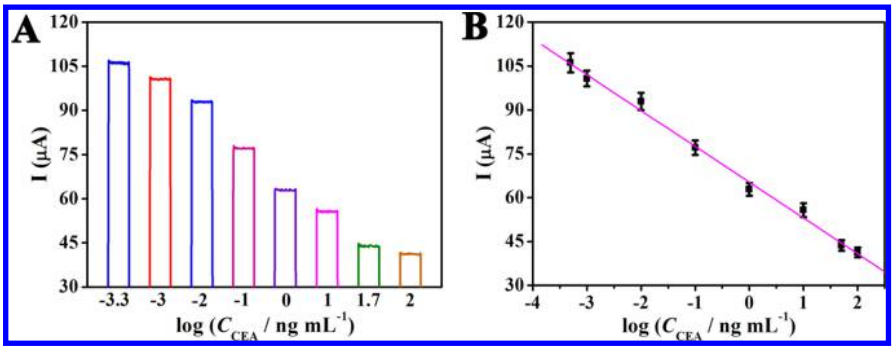

Figure 6. (A) Photocurrent response and (B) calibration curve of the immunoassay for the detection of different concentrations of target Ag from 0.5 pg/mL to 100 ng/mL. The error bars show the standard deviation of five parallel measurements.

also exhibited a wider linear range of detection due to smaller-sized signal labels.

Specificity, Reproducibility, and Stability of the Immunoassay. Specificity is necessary for most of the immunoassays, because nonspecific binding could mislead the detection results. To validate that the photocurrent response of the proposed immunoassay resulted from specific binding of immunoreactions, some of the typical interfering antigens including prostate-specific antigen (PSA), α-fetoprotein (AFP), carbohydrate antigen 19-9 (CA19-9), and carbohydrate antigen 15-3 (CA15-3) were selected for the interference test. As shown in Figure 7, the photocurrent response of the

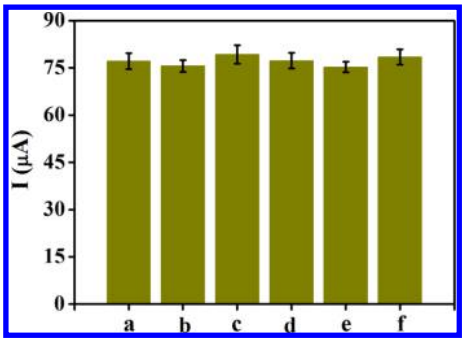

Figure 7. Photocurrent responses of the immunoassay toward 100 pg/mL CEA detection (a) in the absence of interference, or in the existence of 1 ng/mL of (b) PSA, (c) AFP, (d) CA19-9, (e) CA15-3, and (f) their mixture. The error bars display the standard deviation of five parallel determinations.

immunosensor toward 100 pg/mL CEA detection was not affected by PSA, AFP, CA19-9, CA15-3, and their mixture. As compared to the photocurrent response tested without any interfering antigen, the relative deviations of the photocurrent responses measured at the existence of single interfering antigen or their mixture were all within 4.0%. The relative standard deviation (RSD) of five parallel measurements for each interference test was within 3.7%. These results demonstrated that the present immunoassay had a good selectivity with no evident interference coming from nonspecific binding.

The reproducibility of the proposed immunoassay was assessed by relative standard deviations (RSDs) of both within-batch and between-batch. Calculated from the detection results with five parallel tests, the within-batch RSDs were 2.7%, 3.2%, and 3.5% toward 1, 10, and 100 pg/mL of target Ag, respectively. The between-batch RSDs of 3.8%, 3.5%, and 3.1% were obtained by testing the identical samples with five immunosensors prepared separately in the same condition. These results revealed a favorable reproducibility and precision for the present immunoassay.

The stability of the developed immunoassay was evaluated by the degree of photocurrent variation. After the immunosensing electrode was stored in a dark and humid environment at 4 °C for 2 weeks, the photocurrent intensity still retained 94.5% of its starting value, indicating its good long-term storage stability.

CONCLUSIONS

In summary, we established a new, enhanced photoelectrochemical immunosensing platform for ultrasensitive detection of biomarkers based on the cooperation effect of TiO_2/CdSeTe@CdS:Mn sensitization structure and signal amplification of Ab_2−CuS conjugates. As photoelectrochemical matrix of the immunosensing electrode, TiO_2/CdSeTe@CdS:Mn sensitization structure could noticeably enhance the photocurrent thanks to the excellent properties of full absorption of exciting light, ultrafast transfer of electrons, and effective suppression of charge recombination. As signal amplification elements, Ab_2−CuS conjugates could dramatically weaken the photocurrent response due to competitive absorption of exciting light and effective consumption of AA electron donor for the CuS nanocrystals coupled with evident steric hindrance of Ab_2 molecules. Combining the excellent photoelectrochemical property of the TiO_2/CdSeTe@CdS:Mn sensitization structure and the superior signal amplification of the Ab_2−CuS conjugates, the well-established immunosensing platform exhibited an ultralow limit of detection for biomarker detection. Because different antibodies can specifically bind with different biomarkers, the proposed platform has great applied potential in the development of various sensitive photoelectrochemical immunoassays for the detection of low levels of disease-related biomarkers.

ASSOCIATED CONTENT

Supporting Information

The Supporting Information is available free of charge on the ACS Publications website at DOI: 10.1021/acs.analchem.6b00144.

Additional information as noted in text (PDF)

AUTHOR INFORMATION

Corresponding Authors

*E-mail: jrzhang@nju.edu.cn.
*E-mail: jjzhu@nju.edu.cn.

DOI: 10.1021/acs.analchem.6b00144
Anal. Chem. 2016, 88, 3392−3399

*E-mail: yuehe.lin@wsu.edu.

Notes

The authors declare no competing financial interest.

■ ACKNOWLEDGMENTS

We gratefully appreciate the National Natural Science Foundation of China (21375059, 21175065, and 21335004), the National Basic Research Program of China (2011CB933502), and a startup fund of Washington State University.

■ REFERENCES

(1) Haddour, N.; Chauvin, J.; Gondran, C.; Cosnier, S. *J. Am. Chem. Soc.* **2006**, *128*, 9693−9698.
(2) Wang, G. L.; Yu, P. P.; Xu, J. J.; Chen, H. Y. *J. Phys. Chem. C* **2009**, *113*, 11142−11148.
(3) Liang, M. M.; Liu, S. L.; Wei, M. Y.; Guo, L. H. *Anal. Chem.* **2006**, *78*, 621−623.
(4) Wang, G. L.; Xu, J. J.; Chen, H. Y.; Fu, S. Z. *Biosens. Bioelectron.* **2009**, *25*, 791−796.
(5) Chen, K.; Liu, M. C.; Zhao, G. H.; Shi, H. J.; Fan, L. F.; Zhao, S. C. *Environ. Sci. Technol.* **2012**, *46*, 11955−11961.
(6) Zhao, W. W.; Dong, X. Y.; Wang, J.; Kong, F. Y.; Xu, J. J.; Chen, H. Y. *Chem. Commun.* **2012**, *48*, 5253−5255.
(7) Li, W.; Sheng, P. T.; Cai, J.; Feng, H. Y.; Cai, Q. Y. *Biosens. Bioelectron.* **2014**, *61*, 209−214.
(8) Yang, J. J.; Gao, P. C.; Liu, Y. X.; Li, R. X.; Ma, H. M.; Du, B.; Wei, Q. *Biosens. Bioelectron.* **2015**, *64*, 13−18.
(9) Zhao, W. W.; Han, Y. M.; Zhu, Y. C.; Zhang, N.; Xu, J. J.; Chen, H. Y. *Anal. Chem.* **2015**, *87*, 5496−5499.
(10) An, Y. R.; Tang, L. L.; Jiang, X. L.; Chen, H.; Yang, M. C.; Jin, L. T.; Zhang, S. P.; Wang, C. G.; Zhang, W. *Chem. - Eur. J.* **2010**, *16*, 14439−14446.
(11) Li, Y. J.; Ma, M. J.; Zhu, J. J. *Anal. Chem.* **2012**, *84*, 10492−10499.
(12) Zhu, H.; Fan, G. C.; Abdel-Halim, E. S.; Zhang, J. R.; Zhu, J. J. *Biosens. Bioelectron.* **2016**, *77*, 339−346.
(13) Lee, Y. L.; Chi, C. F.; Liau, S. Y. *Chem. Mater.* **2010**, *22*, 922−927.
(14) Pradhan, Narayan.; Sarma, D. D. *J. Phys. Chem. Lett.* **2011**, *2*, 2818−2826.
(15) Bailey, R. E.; Nie, S. M. *J. Am. Chem. Soc.* **2003**, *125*, 7100−7106.
(16) Gurusinghe, N. P.; Hewa-Kasakarage, N. N.; Zamkov, M. *J. Phys. Chem. C* **2008**, *112*, 12795−12800.
(17) Sarma, D. D.; Nag, A.; Santra, P. K.; Kumar, A.; Sapra, S.; Mahadevan, P. *J. Phys. Chem. Lett.* **2010**, *1*, 2149−2153.
(18) Li, P. Q.; Zhang, J.; Wang, H. Y.; Jing, H.; Xu, J. F.; Sui, X. N.; Hu, H. T.; Yin, H. Z. *Catal. Sci. Technol.* **2014**, *4*, 1070−1077.
(19) Yang, J. W.; Wang, J.; Zhao, K.; Izuishi, T.; Li, Y.; Shen, Q.; Zhong, X. H. *J. Phys. Chem. C* **2015**, *119*, 28800−28808.
(20) Zhao, W. W.; Ma, Z. Y.; Yu, P. P.; Dong, X. Y.; Xu, J. J.; Chen, H. Y. *Anal. Chem.* **2012**, *84*, 917−923.
(21) Zhang, X. R.; Liu, M. S.; Mao, Y. N.; Xu, Y. P.; Niu, S. Y. *Biosens. Bioelectron.* **2014**, *59*, 21−27.
(22) Fan, G. C.; Han, L.; Zhang, J. R.; Zhu, J. J. *Anal. Chem.* **2014**, *86*, 12398−12405.
(23) Wang, G. L.; Shu, J. X.; Dong, Y. M.; Wu, X. M.; Li, Z. J. *Biosens. Bioelectron.* **2015**, *66*, 283−289.
(24) Yang, Z.; Chen, C. Y.; Liu, C. W.; Li, C. L.; Chang, H. T. *Adv. Energy Mater.* **2011**, *1*, 259−264.
(25) Balis, N.; Dracopoulos, V.; Bourikas, K.; Lianos, P. *Electrochim. Acta* **2013**, *91*, 246−252.
(26) Zhang, J.; Yu, J. G.; Zhang, Y. M.; Li, Q.; Gong, J. R. *Nano Lett.* **2011**, *11*, 4774−4779.
(27) Zhu, T.; Xia, B. Y.; Zhou, L.; Lou, X. W. *J. Mater. Chem.* **2012**, *22*, 7851−7855.
(28) Yu, X. L.; Cao, C. B.; Zhu, H. S.; Li, Q. S.; Liu, C. L.; Gong, Q. H. *Adv. Funct. Mater.* **2007**, *17*, 1397−1401.
(29) Cai, R.; Chen, J.; Zhu, J. X.; Xu, C.; Zhang, W. Y.; Zhang, C. M.; Shi, W. H.; Tan, H. T.; Yang, D.; Hng, H. H.; Lim, T. M.; Yan, Q. Y. *J. Phys. Chem. C* **2012**, *116*, 12468−12474.
(30) Zhang, S. S.; Zhong, H.; Ding, C. F. *Anal. Chem.* **2008**, *80*, 7206−7212.
(31) Zhang, X. R.; Liu, H. X.; Li, R. J.; Zhang, N. B.; Xiong, Y.; Niu, S. Y. *Chem. Commun.* **2015**, *51*, 6952−6955.
(32) Wang, G. L.; Shu, J. X.; Dong, Y. M.; Wu, X. M.; Zhao, W. W.; Xu, J. J.; Chen, H. Y. *Anal. Chem.* **2015**, *87*, 2892−2900.
(33) Fan, G. C.; Han, L.; Zhang, J. R.; Zhu, J. J. *Anal. Chem.* **2014**, *86*, 10877−10884.
(34) Santra, P. K.; Kamat, P. V. *J. Am. Chem. Soc.* **2012**, *134*, 2508−2511.
(35) Zhu, Y. D.; Peng, J.; Jiang, L. P.; Zhu, J. J. *Analyst* **2014**, *139*, 649−655.
(36) Fan, G. C.; Ren, X. L.; Zhu, C.; Zhang, J. R.; Zhu, J. J. *Biosens. Bioelectron.* **2014**, *59*, 45−53.
(37) Basu, M.; Sinha, A. K.; Pradhan, M.; Sarkar, S.; Negishi, Y.; Govind; Pal, T. *Environ. Sci. Technol.* **2010**, *44*, 6313−6318.
(38) Tian, Q.; Tang, M.; Sun, Y.; Zou, R.; Chen, Z.; Zhu, M.; Yang, S.; Wang, J.; Wang, J.; Hu, J. *Adv. Mater.* **2011**, *23*, 3542−3547.
(39) Gao, J. N.; Li, Q. S.; Zhao, H. B.; Li, L. S.; Liu, C. L.; Gong, Q. H.; Qi, L. M. *Chem. Mater.* **2008**, *20*, 6263−6269.
(40) Chen, H.; Jiang, J. H.; Huang, Y.; Deng, T.; Li, J. S.; Shen, G. L.; Yu, R. Q. *Sens. Actuators, B* **2006**, *117*, 211−218.
(41) Chen, X. J.; Wang, Y. Y.; Zhou, J. J.; Yan, W.; Li, X. H.; Zhu, J. J. *Anal. Chem.* **2008**, *80*, 2133−2140.
(42) Cooper, D. R.; Dimitrijevic, N. M.; Nadeau, J. L. *Nanoscale* **2010**, *2*, 114−121.
(43) Xiong, Z.; Zhao, X. S. *J. Am. Chem. Soc.* **2012**, *134*, 5754−5757.
(44) Yang, Z. J.; Liu, H.; Zong, C.; Yan, F.; Ju, H. X. *Anal. Chem.* **2009**, *81*, 5484−5489.
(45) He, X. L.; Yuan, R.; Chai, Y. Q.; Shi, Y. T. *J. Biochem. Biophys. Methods* **2008**, *70*, 823−829.
(46) Ding, J. W.; Wang, X. W.; Qin, W. *ACS Appl. Mater. Interfaces* **2013**, *5*, 9488−9493.
(47) Liang, K.; Zhai, S. T.; Zhang, Z. D.; Fu, X. Y.; Shao, J. W.; Lin, Z. Y.; Qiu, B.; Chen, G. N. *Analyst* **2014**, *139*, 4330−4334.
(48) Pang, X. H.; Li, J. X.; Zhao, Y. B.; Wu, D.; Zhang, Y.; Du, B.; Ma, H. M.; Wei, Q. *ACS Appl. Mater. Interfaces* **2015**, *7*, 19260−19267.
(49) Zhou, Z. M.; Zhou, J.; Chen, J.; Yu, R. N.; Zhang, M. Z.; Song, J. T.; Zhao, Y. D. *Biosens. Bioelectron.* **2014**, *59*, 397−403.
(50) Lu, W. B.; Qian, C.; Bi, L. Y.; Tao, L.; Ge, J.; Dong, J.; Qian, W. Q. *Biosens. Bioelectron.* **2014**, *53*, 346−354.

DOI: 10.1021/acs.analchem.6b00144
Anal. Chem. 2016, 88, 3392−3399